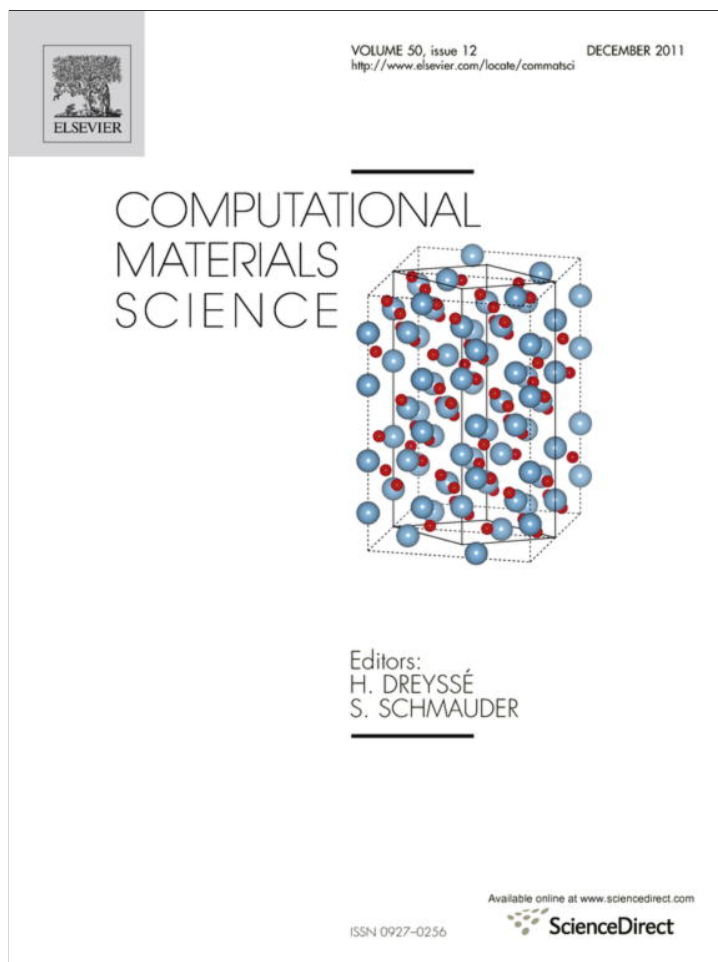


Provided for non-commercial research and education use.
Not for reproduction, distribution or commercial use.



This article appeared in a journal published by Elsevier. The attached copy is furnished to the author for internal non-commercial research and education use, including for instruction at the authors institution and sharing with colleagues.

Other uses, including reproduction and distribution, or selling or licensing copies, or posting to personal, institutional or third party websites are prohibited.

In most cases authors are permitted to post their version of the article (e.g. in Word or Tex form) to their personal website or institutional repository. Authors requiring further information regarding Elsevier's archiving and manuscript policies are encouraged to visit:

<http://www.elsevier.com/copyright>



Contents lists available at ScienceDirect

Computational Materials Science

journal homepage: www.elsevier.com/locate/commatsci

Multiscale simulation of nanometric cutting of single crystal copper and its experimental validation

H.M. Pen^{a,b}, Y.C. Liang^a, X.C. Luo^{b,*}, Q.S. Bai^a, S. Goel^b, J.M. Ritchie^b

^a School of Mechatronics Engineering, Harbin Institute of Technology, Harbin 150001, China

^b School of Engineering and Physical Sciences, Heriot-Watt University, Edinburgh EH14 4AS, UK

ARTICLE INFO

Article history:

Received 8 June 2011

Accepted 4 July 2011

Available online 23 July 2011

Keywords:

Nanometric cutting mechanism

Multiscale simulation

Nano-scratching

Defect structures

Microstructures

ABSTRACT

In this paper a multiscale simulation study was carried out in order to gain in-depth understanding of machining mechanism of nanometric cutting of single crystal copper. This study was focused on the effects of crystal orientation and cutting direction on the attainable machined surface quality. The machining mechanics was analyzed through cutting forces, chip formation morphology, generation and evolution of defects and residual stresses on the machined surface. The simulation results showed that the crystal orientation of the copper material and the cutting direction significantly influenced the deformation mechanism of the workpiece materials during the machining process. Relatively lower cutting forces were experienced while selecting crystal orientation family $\{111\}$. Dislocation movements were found to concentrate in front of the cutting chip while cutting on the (111) surface along the $[\bar{1}10]$ cutting direction thus, resulting in much smaller damaged layer on the machined surface, compared to other orientations. This crystal orientation and cutting direction therefore recommended for nanometric cutting of single crystal copper in practical applications. A nano-scratching experiment was performed to validate the above findings.

© 2011 Elsevier B.V. All rights reserved.

1. Introduction

Single crystal copper has found its wide applications for the fabrication of high accurate instruments and civil communication equipments because of its explicit properties, such as signal transportation and fatigue resistance [1–3]. Nanometric cutting, in which depth of cut is less than 100 nm, is a perfect choice to fabricate microstructures required for such intrinsic products. Nanometric cutting offers nanometer level surface roughness and submicron form accuracy which can meet the demand on high accuracy for these products. In nanometric machining operation, the ratio of cutting edge radius to the depth of cut is larger which is indeed the distinguishing feature compared to conventional machining [4]. On the other hand, some phenomena in nanometric cutting are difficult to observe by experimental means due to the complexity and miniaturization of the cutting process. However, computational simulation method provides an alternative way to accomplish the “on-line” observation of the machining process.

Since the late 1980s Molecular Dynamics (MD) simulation method has been used to study nanometric cutting processes. Ikawa et al. [5] proposed that the sharpness of the diamond tool had a strong influence on the minimum thickness of cut. Maekawa

and Itoh [6] investigated the phenomena of tool wear of a diamond-like tool in micro-machining of single crystal copper. Kim and Moon [7] studied the phenomenon of microcutting with sub-nanometer chip thickness. Kim et al. [8] conducted a three-dimensional MD simulation for AFM-based nano-lithography process which showed that different crystal orientations and ploughing directions had significant influences on the nano-deformation patterns. Liang et al. [9] conducted an integrated MD simulation of scratching and shearing experiments on a single crystal copper specimen. They suggested that the yielding strength of a small-size nanostructure was very sensitive to the imperfection and defect of the copper surface. Zhang et al. [10] simulated the groove fabrication process at atomistic scale using MD method. Results showed that the groove geometry had a huge impact on the groove machining process. In addition, MD method has been extensively applied for the simulation of nanometric cutting, nanoscratching and chemical mechanical polishing processes for other materials, such as silicon, aluminum and multi-layered films [11–14]. However, due to the limitations of computational power, the dimensions of a MD simulation model were usually in the range of few nanometers. Simulation of the full scale of nanometric cutting is still a challenging task.

In recent years, multiscale simulation approach has been developed in the computational materials area. The philosophy of this approach is to retain full atomistic details in the regions of interest

* Corresponding author. Tel.: +44 131 4513197; fax: +44 131 4513129.

E-mail address: x.luo@hw.ac.uk (X.C. Luo).

but uses continuum assumption in the other regions so as to reduce the computational demand. Multiscale method has been used to correlate the mechanical properties of materials with their microstructures [15,16] very little work has been carried out to apply this approach in the study of nanometric cutting. Furthermore, nanometric cutting is basically a multiscale deformation process. The generation, evolution and pile-up of the nanometer level

Table 1

Computational parameters used in simulations.

Parameters	2-D multiscale cutting model
Workpiece material	Copper, EAM potential
Workpiece dimensions	$0.1 \times 0.1 \mu\text{m}$
Tool edge radius	5 nm
Depth of cut	3 nm
Cutting speed	20 m/s
Workpiece orientation	$(001)[\bar{1}10] (001)[100] (110)[001]$ $(110)[\bar{1}10] (111)[\bar{1}10] (111)[211]$

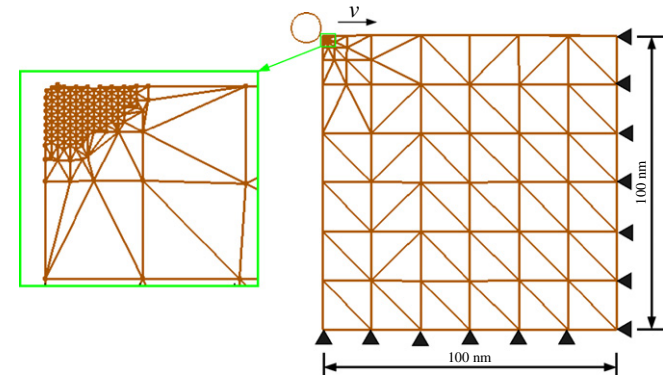


Fig. 1. Multiscale model of nanometric cutting.

dislocations and breakage of the atomic bonds in the cutting region determine the mechanism of nanometric cutting process. It is essential to explore the atomistic mechanism in this region using MD method. The residual stress in the machined surface and sub-surface is a crucial factor for the service performance of the final products. Continuum methods, such as finite element method, can be used to analyze the micro-scale deformation features which are related to the generation of the residual stress. With continuum method the computational time can be saved significantly. In this paper, a multiscale simulation method, Quasicontinuum (QC) [17] was used to study the effect of crystal orientation and the cutting direction on the deformation mechanism in nanometric cutting of single crystal copper.

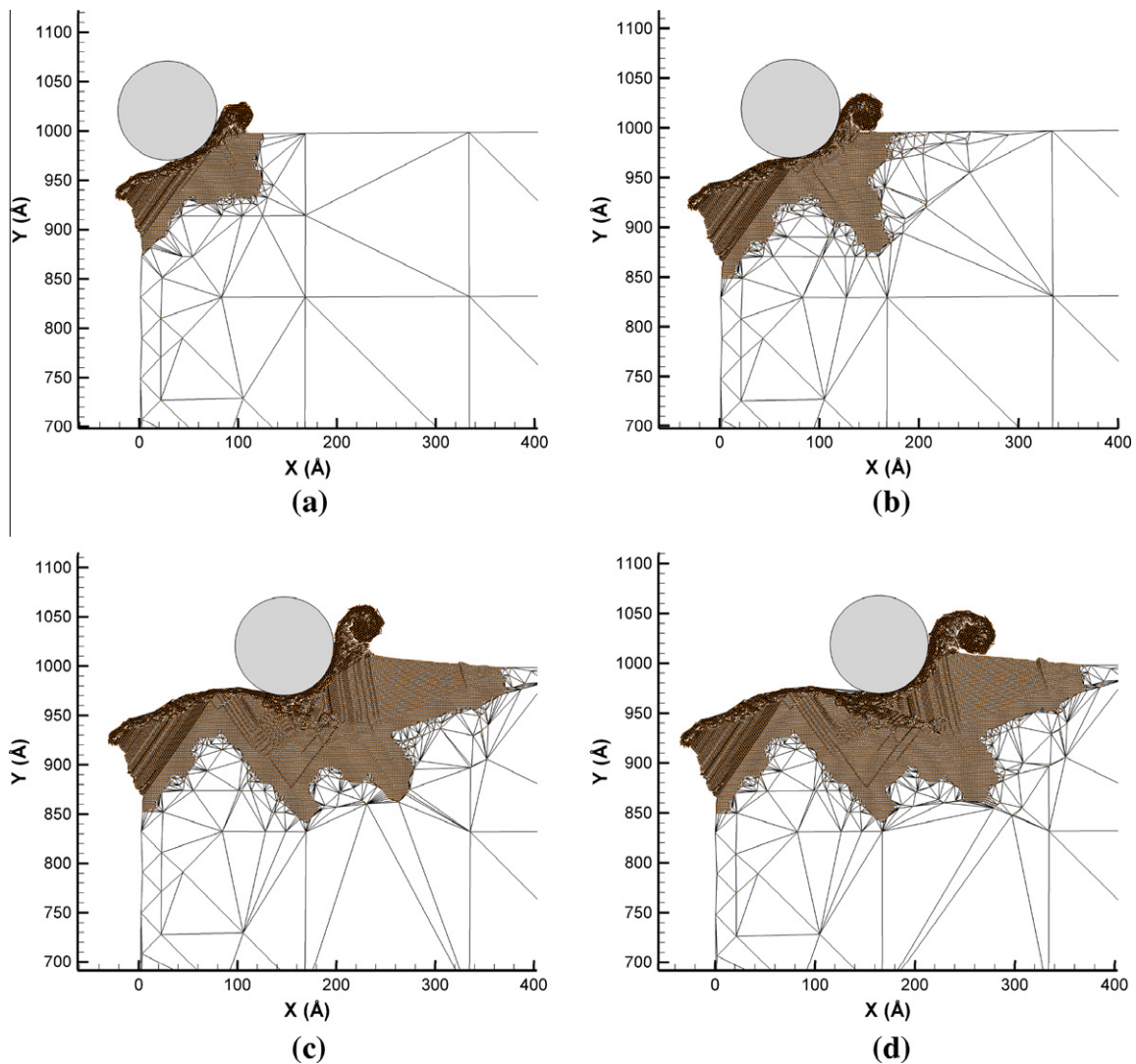


Fig. 2. Snapshots of the multiscale simulation at the cutting distances of 8 nm (a), 12 nm (b), 18 nm (c) and 21 nm (d) in $(001)[\bar{1}10]$ orientation setup.

2. Multiscale simulation model

The multiscale nanometric cutting model is shown in Fig. 1. This model has a plane strain configuration with thickness in the out of plane direction which is equal to the minimal repeat distance in the z direction. Periodic boundary condition was applied in the x and y directions respectively. In this model fix boundary conditions were applied to the nodes in the right and bottom sides of the workpiece. A diamond tool with a cutting edge radius of 5 nm was used to cut the free surface of the workpiece. The region close to the cutting surface was simulated with atomic resolution, while the remaining regions are simulated according to a continuum framework. Finite element nodes were meshed to atomistic size by using the remeshing technology in the cutting region. This multiscale simulation model needs approximately 100 representative atoms against the requirement of 3×10^5 atoms of a similar size atomistic model thus, saves computational time. In this study six setups of the crystal orientation of the copper workpiece and the cutting direction were chosen to be adopted in the simulation in order to study their effects on the machining mechanism. The process parameters used in the simulations were summarized in Table 1.

3. Simulation results and discussions

3.1. The analysis of material removal mechanism

3.1.1. (001) orientation and $[\bar{1}10]$ cutting direction setup

Fig. 2 shows the workpiece deformation under different time steps during the nanometric cutting process when the (001) workpiece surface was cut along the $[\bar{1}10]$ direction. It could be seen that when the tool advanced towards the workpiece, the workpiece began to deform. The workpiece material atoms would be rearranged when the strain energy reserved in the deformed lattice was larger than the binding energy of the workpiece atoms. On the other hand, when the primary shear stress generated by the intrusion action of the cutting tool was larger than the critical shear stress of single crystal copper, dislocation slips would be generated in the lattices to release the strain energy (as shown in Fig. 2a). There were more dislocations generated as the tool advances. Because of the intrusion and the shear action of the tool, some dislocations moved forward along the tool rake face and gradually formed a chip. Some dislocations moved along the lower left side and flew back to the workpiece bulk to form the machined surface as the tool passed by. Meanwhile, elastic recovery occurred

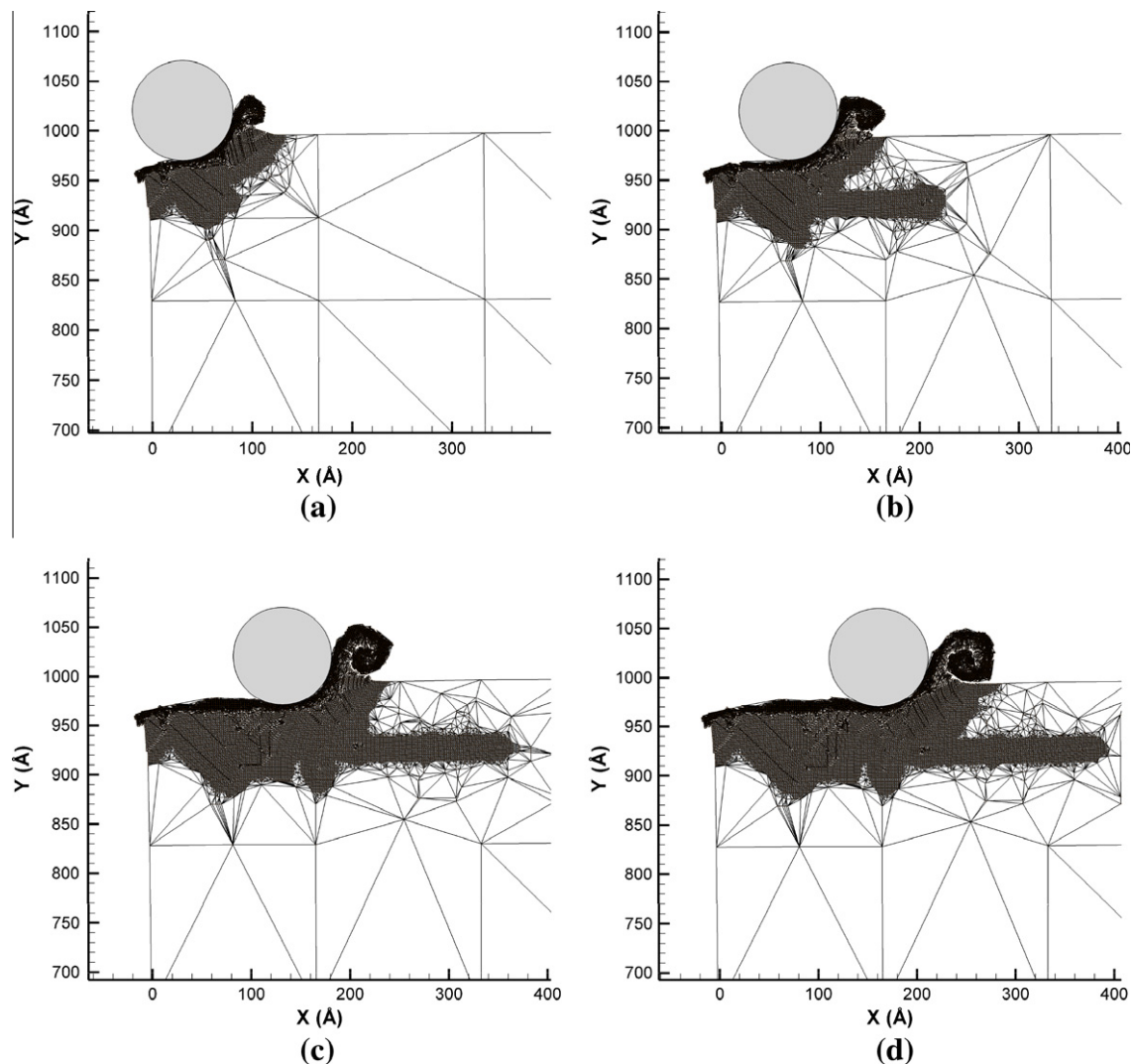


Fig. 3. Snapshots of the multiscale simulation at the cutting distances of 8 nm (a), 12 nm (b), 18 nm (c) and 21 nm (d) in the (001)[100] orientation setup.

in the machined surfaces. At this time, majority of dislocations disappeared, but one portion of dislocation slid and emerged in the machined surface. The emergence of dislocations caused an uneven surface, which could be called the surface roughness in the nanometric cutting progress. As shown in Fig. 2c, there were still some dislocations remained in the bulk of workpiece and formed a deformation layer. The above analysis unveiled the basic deformation mechanism in nanometric cutting of single crystal copper. However, under different combinations of crystal orientation and cutting directions the deformation process will show different characteristics in various aspects such as generation and evolution of dislocations and surface recovery. These differences will be discussed in the following sessions.

Due to the intrusion action of the tool edge, the slip plane ($\bar{1}11$) activated continuously, thus the generated dislocations continued to move forwards and backwards. Some dislocations moved backward to the bulk of the workpiece surface and appeared underneath the machined surface which aroused a large plastic deformation near the initial cutting point, as shown in Fig. 2a. Some dislocations moved forwards along the slip planes with an angle of 55° to the cutting direction across the shear area and eventually disappeared on the free surface. At this time, the materials were removed and chips are generated. But there were no obvious shear band observed. The main reason was that the

movement of dislocations was not exactly along the slip planes but along a bended direction due to the intrusion action of the tool cutting edge.

As the tool advanced, the workpiece materials in the lower right side of the contact region between the tool and the workpiece slipped along the slip plane ($\bar{1}11$) which has an angle of about -55° to the cutting direction. Surface elastic recovery occurred as these dislocation slips moved backwards. At the same time, new dislocation slips were generated along the slip plane ($\bar{1}11$). These dislocations moved below the workpiece surface and generated jogs. Many dislocation reactions like this could be observed to take place on the bottom of the tool cutting edge. The jogs or kinks generated by these dislocation reactions would block the successive movement of dislocations. Since the dislocation movement remained confined, the crystal lattice below the tool edge deformed severely (as shown in Fig. 2c). It can be seen from Fig. 2c–d that the dislocations which have a jog reaction showed no obvious movement after a cutting distance of 3 nm. A lot of jogs reactions and the intrusion of tool caused the subsurface hardening.

Fig 2c–d also indicates that the angle between the cutting direction and the slip planes in the front of the tool became large and the crystal lattices of material rotated. This meant that the material had a whole deformation under the intrusion action of the cutting tool.

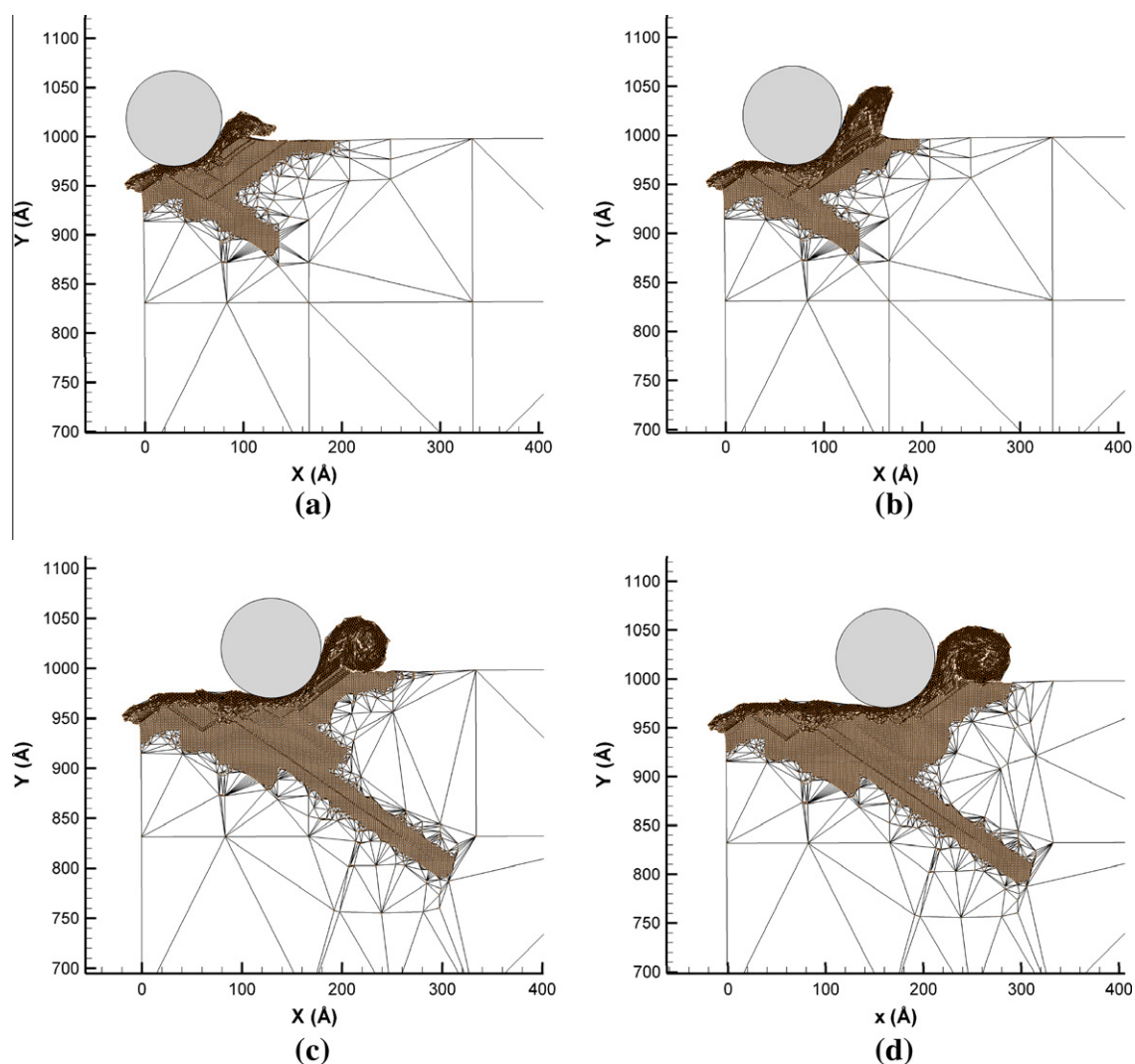


Fig. 4. Snapshots of the multiscale simulations at the cutting distances of 8 nm (a), 12 nm (b), 18 nm (c) and 21 nm (d) in the $(110)[001]$ orientation setup.

3.1.2. (0 0 1) orientation and [1 0 0] cutting direction setup

Fig. 3 shows the workpiece deformation under different cutting distances during the nanometric cutting process when the (0 0 1) surface was cut along the [1 0 0] direction. There were dislocations emitted in the subsurface and in front of the tool cutting edge. But there was no obvious piled deformation like that appears under the (0 0 1)[$\bar{1}$ 1 0] setup. This phenomenon indicated that the material is not amendable to machining using this combination of crystal orientation and cutting direction.

3.1.3. (1 1 0) orientation and [0 0 1] cutting direction setup

Fig. 4 shows the workpiece deformation under different time steps during the nanometric cutting process when the (1 1 0) surface was cut along the [0 0 1] direction. The dislocations emitted along the slip surface (11 $\bar{1}$) soon after the contact of the tool edge and the workpiece. Due to a short cutting distance, these dislocations moved across the shear zone and went out of the surface of the workpiece and formed steps which resulted in the generation of the cutting chips. These slip planes had an angle of around 35° to the cutting direction which indicated a phenomenon of shear bank like traditional cutting. This meant that the deformation of the workpiece was mainly based on the shear action in this orientation setup. As the tool advanced, some dislocations emitted along the slip plane (1 1 1), as shown in Fig. 4a. The

dislocations which emitted along an angle of around 35° to the cutting direction move towards the shear zone and help to remove the materials although few of them moved backwards. This type of shear band made the intrusion action of the tool cutting edge to be released timely, so the cutting action had a little effect on the deformation ahead of the chip. Dislocations along the plane (1 1 1) emit and move deep into the workpiece with further advancement of the tool. From Fig. 4d, it could be seen that the dislocation length increased up to a length of 17 nm as there was no restriction on the other slip planes. A thickness of 0.5 nm of elastic recovery layer in the machined surface was observed under this orientation and cutting direction setup.

3.1.4. (1 1 0) orientation and [$\bar{1}$ 1 0] cutting direction setup

Fig. 5 shows the workpiece deformation during the nanometric cutting process when the (1 1 0) surface was cut along the [$\bar{1}$ 1 0] direction. The cutting chip started to generate soon after the cutting action took place. There was little plastic deformation near the initial cutting point. This deformation mechanism was similar to that observed under the (0 0 1)[1 0 0] setup. The reason was that the {1 1 1}-type planes were precluded in these two orientations due to the application of plane strain conditions in this multiscale cutting model. It also resulted in the plastic deformation because of the climb of the dislocations which indicated that the cutting

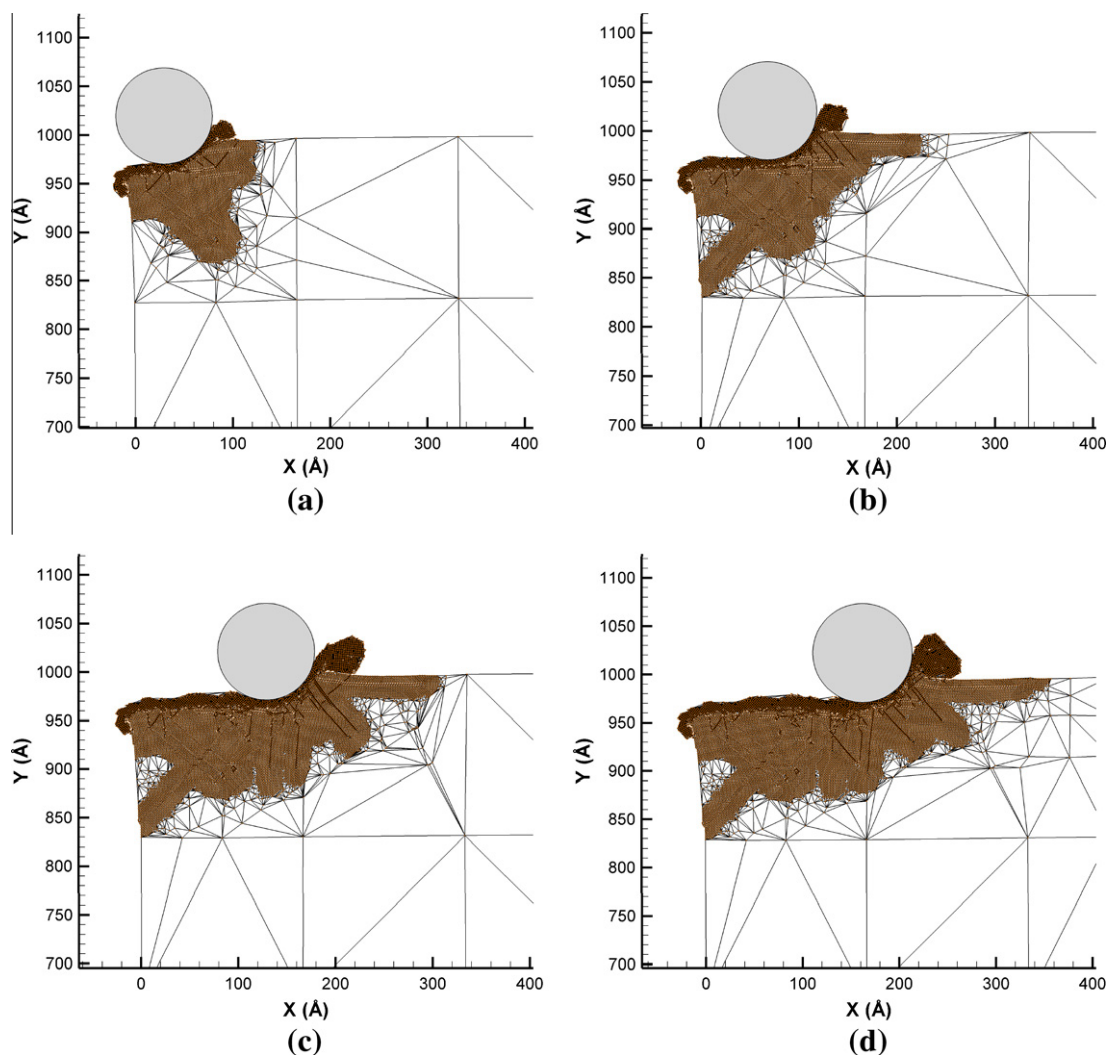


Fig. 5. Snapshots of the multiscale simulation at the cutting distance of 8 nm (a), 12 nm (b), 18 nm (c) and 21 nm (d) in the (1 1 0)[$\bar{1}$ 1 0] orientation setup.

action was not stable when the material properties were changed because of the confinements from the grain boundary, dislocation lock and impurity in the workpiece materials.

3.1.5. (1 1 1) orientation and $[\bar{1} 1 0]$ cutting direction setup

Fig. 6 shows the workpiece deformation under different time steps during the nanometric cutting process when the (1 1 1) surface was cut along the $[\bar{1} 1 0]$ direction. Under this combination the cutting direction remained parallel to the slip planes of the single crystal copper. After the initial contact of the tool and the workpiece, crystal slips were generated in the two layers near the surface of the workpiece along the slip plane (1 1 1). The partial dislocations emitted forwards quickly. The atoms contacting with the tool rake face were intruded out to form the cutting chip, as shown in Fig. 6a. When these partial dislocations emitted to some extent, distorted deformation took place at a place of 15 nm from the tool rake face. This deformation caused a blow-up in the surface of the workpiece, which prohibited the evolution of the dislocations moving forwards. After that, new partials emitted along the (1 1 1) slip plane, which resulted in parts of workpiece appeared above this slip plane and moved forwards. This phenomenon could be seen in Fig. 6b. As the cutting loads increased, some atoms ahead of the tool rake face moved up due to the intrusion of the cutting tool. This movement blocked the continuous evolution of the partial dislocations.

From the deformation plots, it can be seen that the deformation of workpiece concentrated mainly near the contact region between the tool edge and the workpiece. There was no obvious generation of dislocation in the machined surface and subsurface. This would contribute to a good surface integrity.

3.1.6. (1 1 1) orientation and $[\bar{2} 1 1]$ cutting direction

Fig. 7 shows the workpiece deformation under different time steps during the nanometric cutting process when the (1 1 1) surface was cut along the $[\bar{2} 1 1]$ direction. Similar to earlier observation on the (1 1 1) $[\bar{1} 1 0]$ orientation setup, the partial dislocations emitted along the (1 1 1) slip plane near the contact region soon after the tool advanced. But under this orientation setup only partial dislocations along the (1 1 $\bar{1}$) slip plane were activated. The dislocations on the finished surface slipped along the direction of 70° to the cutting direction which tended to move towards the subsurface. On the other hand, dislocations moved upwards in the shear zone. Shear band could be seen similar to the earlier observation on the (1 1 0) $[0 0 1]$ orientation setup. Under a cutting distance of 20 nm, the deepest dislocation had already moved to a position of 13 nm from the machined surface. The distinguishing feature of the cutting process from the (1 1 1) $[\bar{1} 1 0]$ orientation was that the dislocations along the (1 1 1) plane had moved to a position of 55 nm away from the tool rake face. The main reason for this phenomenon was that the dislocations could move forward because a

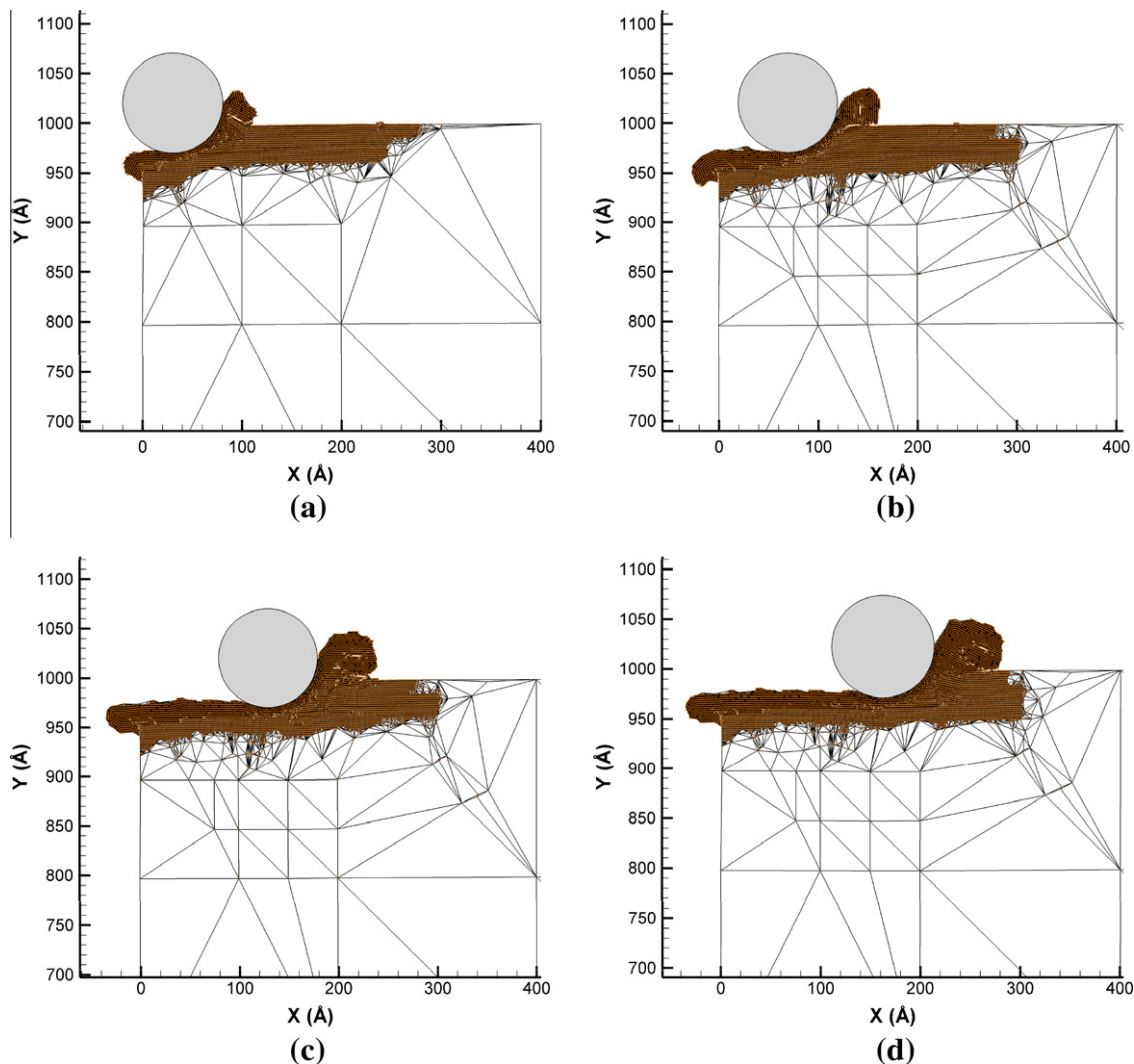


Fig. 6. Snapshots of the multiscale simulation at the cutting distance of 8 nm (a), 12 nm (b), 18 nm (c) and 21 nm (d) in the (1 1 1) $[\bar{1} 1 0]$ orientation setup.

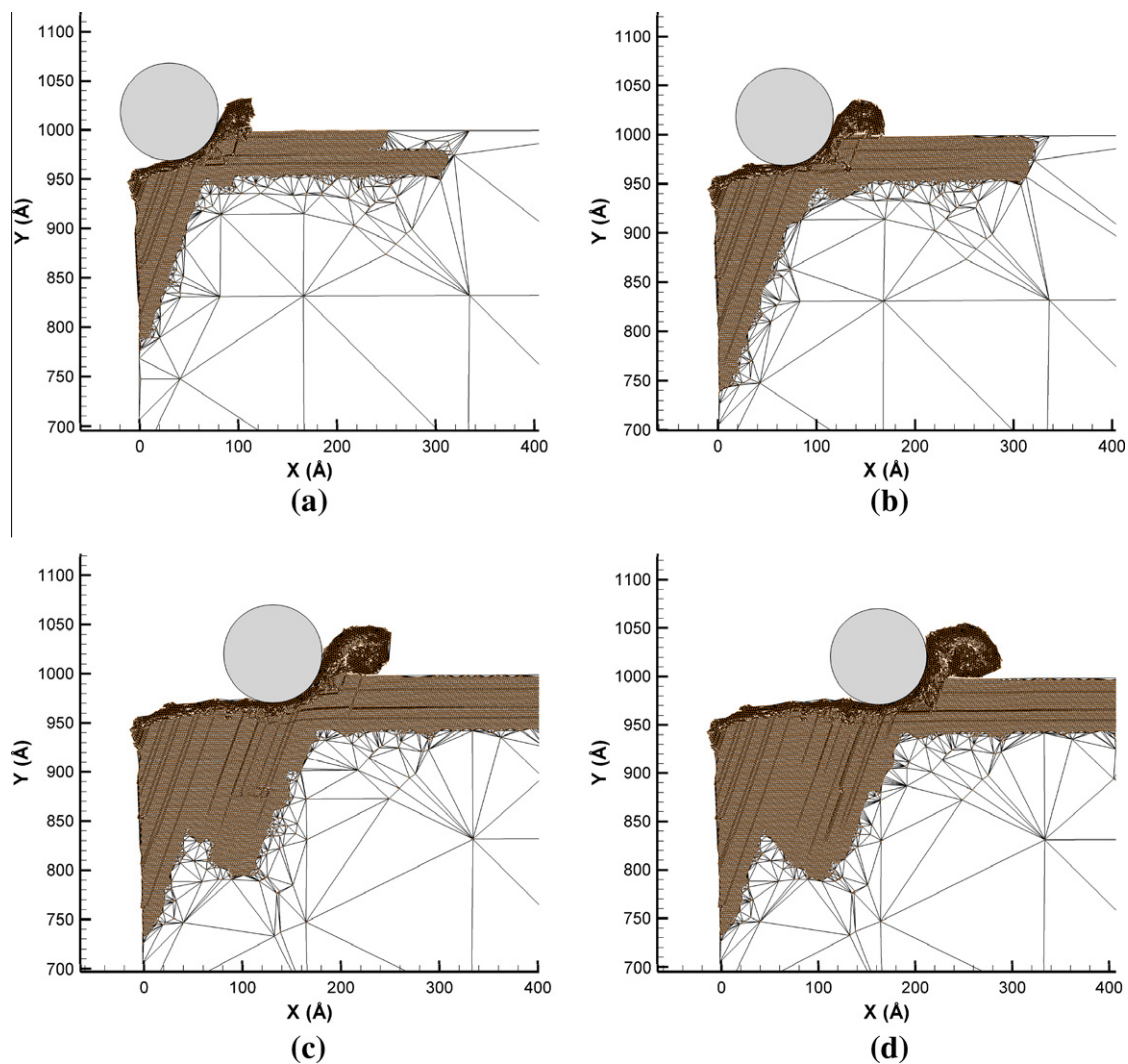


Fig. 7. Snapshots of the multiscale simulation at the cutting distance of 8 nm (a), 12 nm (b), 18 nm (c) and 21 nm (d) in the $(111)[211]$ orientation setup.

part of energy could be released by the $(11\bar{1})$ slip plane after the dislocations moved to some extent. Similar to the other orientations setups above, there occurred elastic recovery on the machined surface as the tool passes by.

3.2. Cutting forces and friction coefficients

3.2.1. Cutting forces

Fig. 8 shows the variation of cutting forces for a combination of $(001)[100]$ orientation. The forces were found to be stable at about a cutting distance of 3 nm. The normal cutting force remained larger than the tangential force. This meant that the tool had a large intrusion action to the workpiece. The fluctuations of the cutting forces were caused by the generation and evolution of the dislocations.

Fig. 9 represents the average tangential cutting forces F_x , normal cutting forces F_y and resultant forces F_s at different crystal orientations and cutting directions setups. The cutting force was obtained as an average value among 10–20 nm cutting distance. The value of F_x was found to be relatively lower in the $(111)[211]$ orientation setup followed by $(111)[\bar{1}10]$ combination. This indicated that the F_x in the crystal orientation family $\{111\}$ remained lower compared to those in the $\{100\}$ and $\{110\}$ crystal orientation families. This conclusion is consistent

with the theory suggesting that low tangential cutting force should be observed in the easiest slip plane in the Fcc type materials (i.e. $(111)[110]$).

3.2.2. Average friction coefficients

Fig. 10 shows the ratio of F_x to F_y under different orientation setups. This ratio could be defined as friction coefficient between the workpiece and the tool. It could be seen that the friction coefficients were all above 0.55 under the orientation setups.

3.3. The distribution of residual stress in the machined surface

Fig. 11 shows the distribution of Von Mises equivalent stress at six different crystal orientations and cutting directions setups when the cutting distances reached 20 nm. High stress values were observed in the regions of the dislocation emission. This meant that the workpiece materials deformed severely near the dislocations. The simulation results showed that under these orientation setups the effective stress in the cutting region were all higher than 10 GPa. This value was in excellent agreement with the earlier reported value by Liang et al. [17]. Since the theoretical yield strength of the single crystal copper (9.73 GPa) [18], was lower than this value, it helped to break the bonds of the copper atoms and removed the materials.

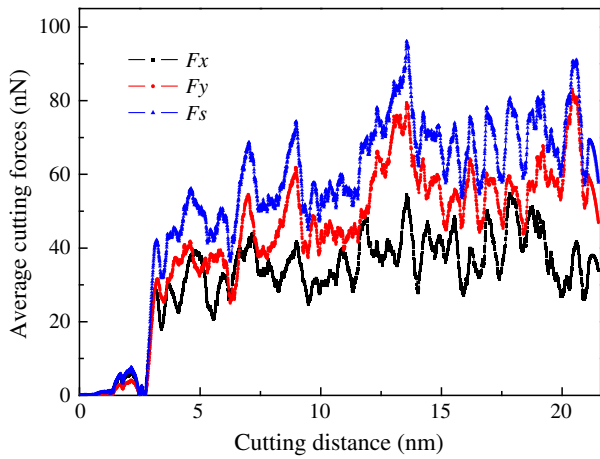


Fig. 8. The variation of the cutting forces with the cutting distances in the (001)[100] orientation.

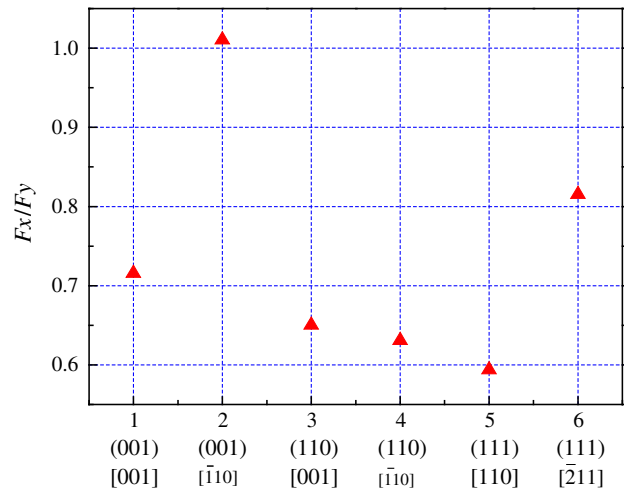


Fig. 10. The values of F_x/F_y at different orientation setups.

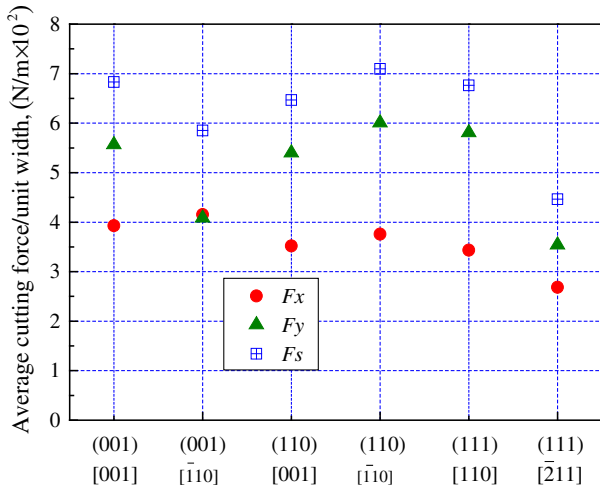


Fig. 9. The variations of the cutting forces at different orientation setups.

Comparing Fig 11 a to b, it could be seen that the stress layer remained thinner under the (111) $\bar{1}10$ orientation setup which was an indication of minimal subsurface damage using this orientation setup.

4. Experimental validation

4.1. Nano-scratching experiments

Nano-scratching experiments were carried out to emulate the nanometric cutting process and validate the multiscale simulation. The material of the single crystal copper was prepared by the Bridgeman method. Its crystal orientation was determined by an X-ray orientation device (YX-2). The crystal orientations and cutting directions used in the experiments were shown in Fig. 12. The sample material was cut into six rectangle blocks of $10 \times 10 \times 3$ mm (in length, width and height). The surface of the copper specimens was polished to remove surface residual stresses before the nano-scratching experiments.

The nano-scratching experiment was performed on a Hysitron Tribolindenter on which a conical indenter with a $1 \mu\text{m}$ tip radius was used. During the experiment the ambient temperature was kept at 20°C . Six scratching experiments were carried out on each

specimen by using six different loads (100, 400, 700, 1000, 1300 and $1600 \mu\text{N}$ respectively) as per the multiscale simulations.

4.2. Experimental results

Fig. 13 represents the surface topography of the single crystal copper at different orientation setups after the nano-scratching experiments under a normal load of $1000 \mu\text{N}$. It could be seen that there were side flows to some extent on both sides of furrows. A lot of pile-ups were observed ahead of the furrows. Obvious differences were observed in terms of the directions and heights of the side flows and pile-up ahead of the furrows under different orientation setups. This phenomenon may have been caused by the fact that the different patterns of dislocation slips were in existence under the different orientation setups which in principle determined the level and format of plastic deformation of the single crystal copper in nanometric cutting.

Fig. 14 represents the variation of the tangential forces under different scratching depths. It can be seen that the tangential forces increased with the increment of the cutting depths. The tangential forces remain almost the same value when scratching the (001) and the (110) faces of the copper specimens. However, the tangential forces for scratching the (111) face of the copper specimen were much smaller than those measured in scratching the (001) and the (110) faces which were consistent with the simulation results. The variation of the tangential cutting forces in different orientation was also consistent with the experimental results obtained by ultra precision diamond turning experiment [19].

Fig. 15 represents the variation of the friction coefficients under different normal loads. It could be seen that the friction coefficients showed an obvious increase with the rise of the normal loads when the loads were lower than $700 \mu\text{N}$. When the normal loads were larger than $1000 \mu\text{N}$, the friction coefficients became stable. The value of friction coefficient remained lower while using (111) $\bar{1}10$ orientation leading to good surface quality which was again consistent with the simulation result.

5. Conclusions

In this paper QC method was utilized to build a multiscale model for nanometric cutting of single crystal copper. The resulting chip morphology, generation and evolution of defects, residual stresses and cutting forces were analyzed under different crystal orientations and cutting directions which were validated by nano-scratching. The following conclusions can be drawn:

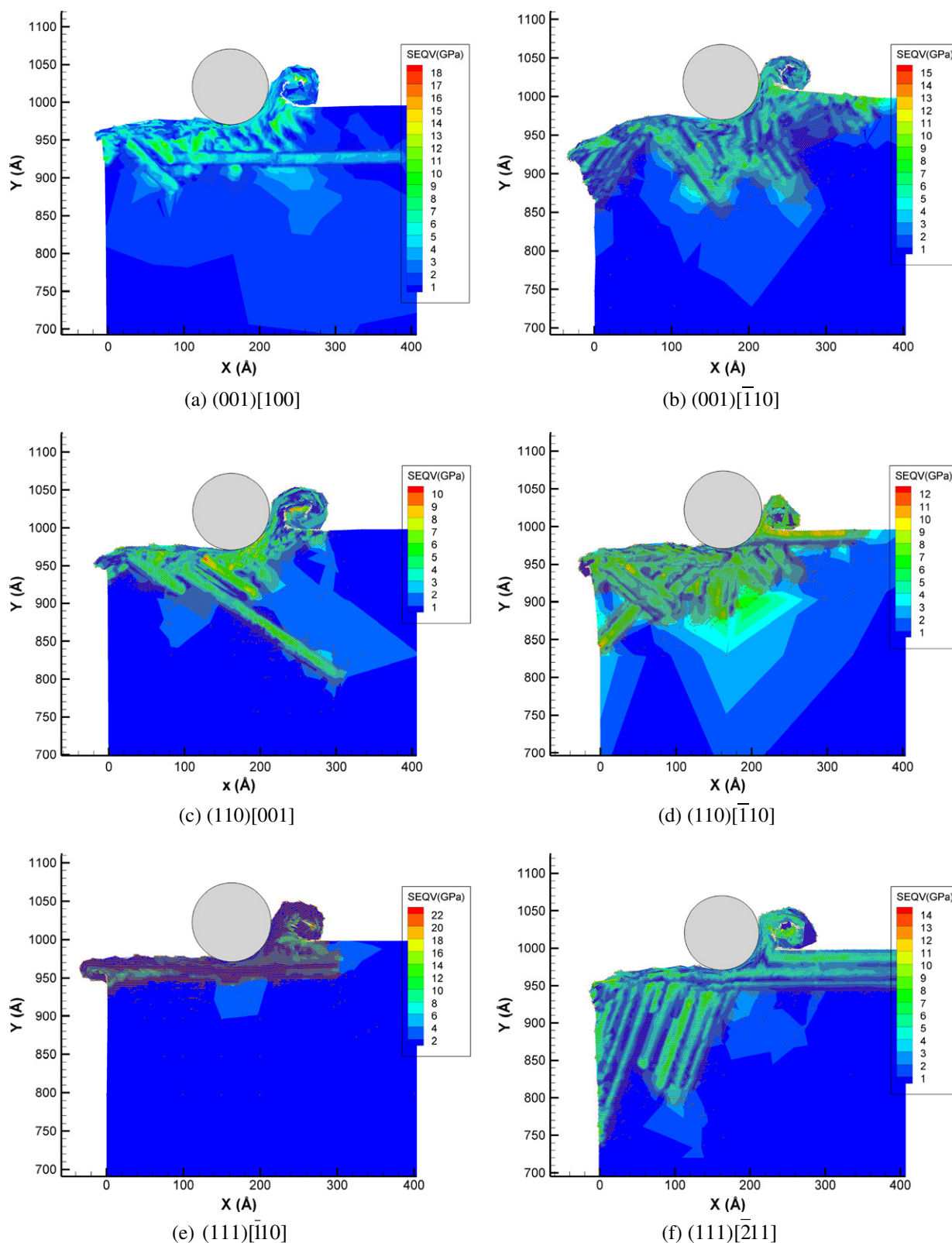


Fig. 11. Contour distribution of Von Mises equivalent stress at cutting distance of 20 nm. Units: coordinates Å and contour plots GPa.

1. The crystal orientations of the copper workpiece and the cutting directions have a pronounced effect on the nanometric cutting mechanism. For the $(001)[\bar{1}10]$ orientation setup, the $(\bar{1}11)$ and the $(1\bar{1}1)$ slip planes were found to be activated. The dislocations emitted on these two slip planes reacted to form jogs or kinks, which prohibited the dislocation movement. Under the

intrusion action of the tool cutting edge, the machined surface became hard. At the same time, the workpiece material lattices rotate with further advance of the tool cutting edge. In the $(110)[001]$ orientation setup, a lot of dislocations with around 35° to the cutting direction were generated and a shear band like traditional cutting was formed. In the $(111)[\bar{1}10]$

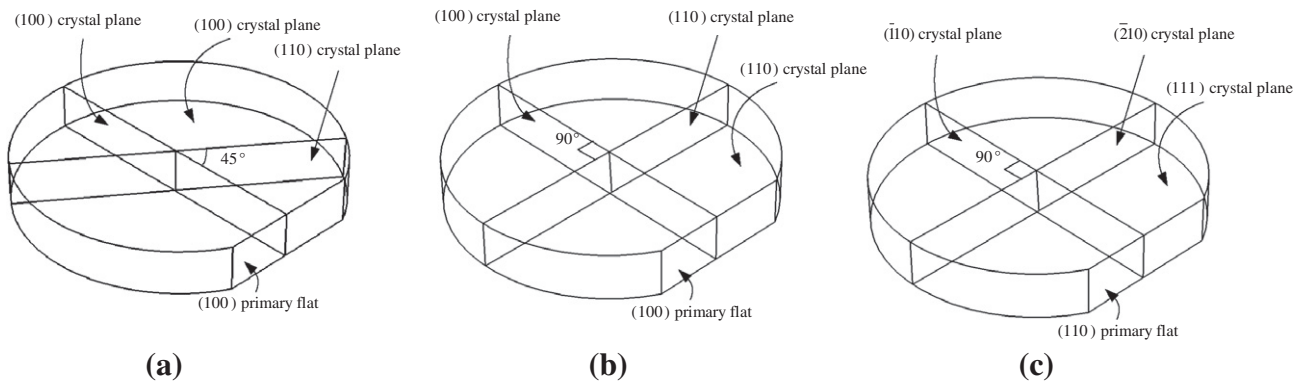


Fig. 12. Schematic diagram of the different orientations and directions setup used in the nano-scratching: (a) (1 0 0), (b) (1 1 0) and (c) (1 1 1).

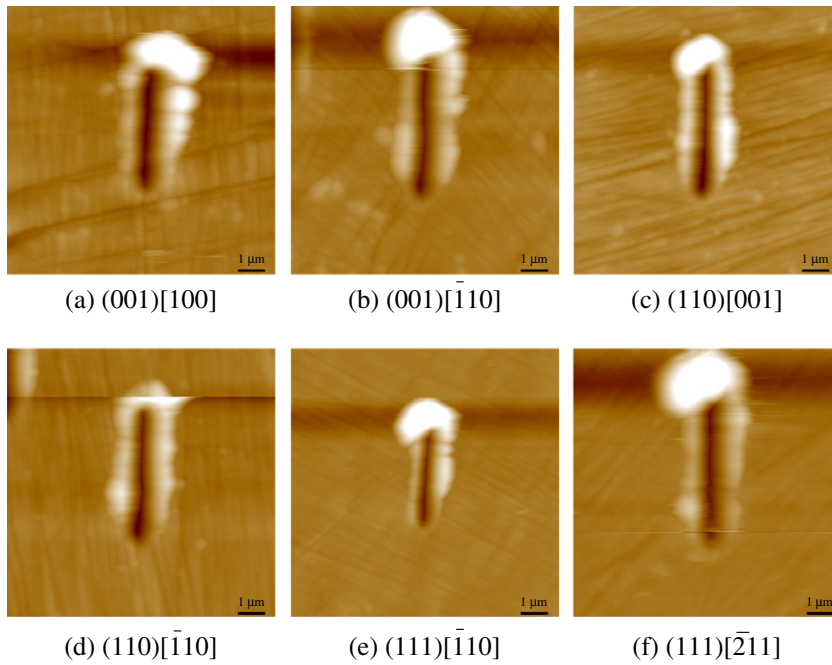


Fig. 13. Surface topography of the single crystal copper at different orientation setups obtained in the nano-scratching.

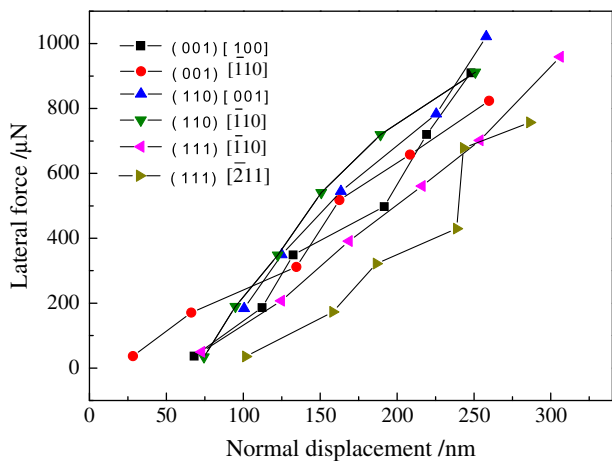


Fig. 14. Normal displacements under different normal loads in the nano-scratching.

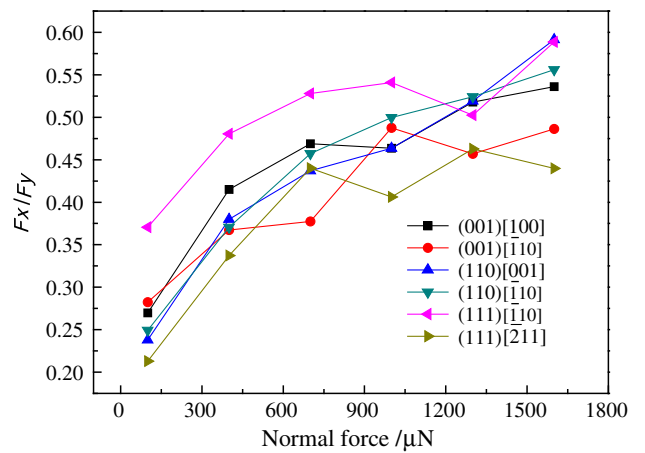


Fig. 15. The friction coefficients under different normal loads in the nano-scratching.

orientation setup, the generations and reactions of the dislocations concentrated in the front of the chip. There were few dislocations evolution towards to the machined surface resulting in a thinner damaged layer in the machined surface. In the $(111)[211]$ orientation setup, the $(11\bar{1})$ and the (111) slip planes were found to be activated resulting in smooth movement of the dislocation ahead of tool.

- The tangential cutting force had the smallest value in the crystal orientation family $\{111\}$. The cutting forces in the $\{100\}$ and $\{110\}$ crystal orientation families were almost the same. The cutting force and friction coefficients obtained in the multiscale simulation were consistent with the results obtain from the nano-scratching experiments.
- Residual stress analysis showed that there exists a high value of stress in the regions of dislocations. The distributions of the residual stress in the machined surface were quite different under different orientation setups. The thinnest deformation layer was observed when $(111)[\bar{1}10]$ orientation was used. This indicates that the $(111)[\bar{1}10]$ orientation setup is the most amendable to machining for practical purposes and thus, recommended.
- Multiscale simulation methodology is much efficient to study nanometric turning process compared to the classical molecular dynamic simulation model.

Acknowledgements

The authors would like to thank the financial supports from National Science Foundation for Distinguished Young Scholars of

China (Project No. 50925521), the National Nature Science Foundation of China (Project No. 50705023) and Scotland–China Higher Education Research Partnership for PhD Studies (Project No. 112978).

References

- A. Ohno, *J. Met.* 38 (1986) 14–16.
- Z.M. Xu, J.G. Li, J.S. Li, H.Z. Fu, *Chin. J. Nonferrous Metals* 9 (1999) 577–581.
- Y.T. Ding, G.J. Xu, F.W. Guo, S.Z. Kou, *Chin. J. Nonferrous Metals* 13 (2003) 1071–1076.
- X. Luo, K. Cheng, X. Guo, R. Holt, *Int. J. Prod. Res.* 41 (2003) 1149–1165.
- N. Ikawa, S. Shimada, H. Tanaka, G. Ohmori, *Ann. CIRP* 40 (1991) 551–554.
- K. Maekawa, A. Itoh, *Wear* 188 (1995) 115–122.
- J.-D. Kim, C.-H. Moon, *J. Mater. Process. Technol.* 59 (1996) 309–314.
- Y.S. Kim, K.H. Na, S.O. Choi, S.H. Yang, *J. Mater. Process. Technol.* 155–156 (2004) 1847–1854.
- Y.C. Liang, J.X. Chen, M.J. Chen, Y.L. Tang, Q.S. Bai, *Comput. Mater. Sci.* 43 (2008) 1130–1140.
- J.J. Zhang, T. Sun, Y.D. Yan, Y.C. Liang, S. Dong, *Appl. Phys. A* 94 (2009) 593–600.
- F.Z. Fang, H. Wu, Y.C. Liu, *Int. J. Mach. Tools Manuf.* 45 (2005) 1681–1686.
- X.S. Han, Y.Z. Hu, S.Y. Yu, *Appl. Phys. A* 95 (2009) 899–905.
- R. Komanduri, N. Chandrasekaran, L.M. Raff, *Ann. CIRP* 48 (1999) 67–72.
- Te-Hua Fang, Chien-Hung Liu, Siu-Tsen Shen, S.D. Prior, Liang-Wen Ji, Jia-Hung Wu, *Appl. Phys. A* 90 (2008) 753–775.
- R.E. Miller, E.B. Tadmor, *J. Comput. Aided Mater. Des.* 9 (2002) 203–239.
- W.K. Liu, E.G. Karpov, S. Zhang, H.S. Park, *Comput. Methods Appl. Mech. Eng.* 193 (2004) 1529–1578.
- Y.C. Liang, H.M. Pen, Q.S. Bai, *Acta. Metall. Sin.* 45 (2009) 1205–1210.
- H.Y. Liang, X.G. Ni, X.X. Wang, *Acta. Metall. Sin.* 37 (2001) 833–836.
- S. To, Effect of crystallographic orientation on material behaviour in ultraprecision diamond turning of single crystals, The Hong Kong Polytechnic University, 2000.